THE ASTROPHYSICAL JOURNAL, 335:584–592, 1988 December 15

MOLECULES AT EARLY EPOCHS. III. THE LYMAN-ALPHA DISK SYSTEM TOWARD 1331+170[1]

FREDERIC H. CHAFFEE, JR.
Multiple Mirror Telescope Observatory
JOHN H. BLACK
Steward Observatory
AND
CRAIG B. FOLTZ
Multiple Mirror Telescope Observatory
Received 1988 March 17; accepted 1988 June 1

ABSTRACT

We present high signal-to-noise spectroscopic observations of the $z = 1.776$ absorption system toward the QSO MC 1331+170. The system contains strong H I Lyα absorption characteristic of the so-called "Lyman-α disk" systems from which a neutral hydrogen column density of 1.5×10^{21} cm^{-2} is inferred. Data on lines of C, Si, Fe, O, Mg, and Al at the Lyα and 21 cm redshift are presented, and the existence of detectable absorption by C and Si in several states of ionization allows us to construct a range of simple physical models for the absorbing cloud.

The most plausible of these suggest matter and energy densities in the $z = 1.776$ cloud similar to those found in Galactic diffuse interstellar clouds: density $n_H \approx 10$–3000 cm^{-3} and an ultraviolet radiation field 0.1–50 times as intense as mean Galactic starlight. The metal-to-hydrogen ratio in the gas is found to be of the order of 0.05 times the solar value.

The lines of the Lyman and Werner systems of molecular hydrogen lie below the atmospheric limit and cannot be observed from the ground. We synthesize the H_2 spectrum and predict that if its column density exceeds 10^{14} cm^{-2} it should be detectable with the Space Telescope and would provide further constraints on physical conditions in the cloud, especially with respect to the dust-to-gas ratio and the temperature.

We search unsuccessfully for absorption by carbon monoxide and infer that its abundance relative to that of neutral, atomic hydrogen is at least one order of magnitude lower than that found in diffuse or thick Galactic interstellar clouds. Because of the complexities of the CO photochemistry, however, this limit does not provide a useful constraint on our models.

Subject headings: abundances — cosmology — galaxies: intergalactic medium — quasars

I. INTRODUCTION

The existence of molecular absorption toward high-redshift QSOs has been addressed inconclusively in the literature for more than a decade. Aaronson, Black, and McKee (1974) first presented evidence for possible H_2 absorption in a cloud of high column density at $z = 2.309$ toward PHL 957, and more recently Varshalovich and Levshakov (1982) summarized the state of possible molecular identifications toward QSOs.

Although the majority of these efforts have been aimed at detecting H_2, Levshakov, Khersonskiĭ, and Varshalovich (1986) suggested absorption features from carbon monoxide might be seen toward PHL 61 and toward other QSOs with large H I column densities.

The present paper is the third in a series aimed at addressing the question of molecular absorption at earlier epochs in light of the better data now available and the more sophisticated analysis of such data now possible. Chaffee, Foltz, and Black (1986, hereafter Paper I) searched for redshifted ultraviolet lines of CO toward PHL 61 and found no evidence for its presence. We showed that no significant neutral hydrogen absorption exists along the line of sight to PHL 61 and suggested that only when such an absorber has a neutral hydrogen column density, N(H), in excess of $\approx 10^{19}$ cm^{-2} might detectable amounts of CO be produced. We also suggested that molecular searches concentrate on lines of sight that exhibit damped H I Lyman α absorption profiles such as those that arise in the "Lyman α disk systems" described by Wolfe *et al.* (1986).

In order to reexamine the question of H_2, Black, Chaffee, and Foltz (1986, hereafter Paper II) obtained high signal-to-noise (S/N) data of the $z = 2.309$ cloud toward PHL 957. The lines of the Lyman and Werner systems of H_2 most likely to be detectable toward QSOs lie near or below the Lyβ line of H I and hence are invariably buried in the underbrush of the Lyα forest. In Paper II we demonstrated that in conditions likely to exist at these epochs, molecular hydrogen in amounts similar to those that arise in Galactic interstellar clouds would produce a forest of its own, and suggested that past efforts to detect H_2 from wavelength coincidences with lines of the Lyman and Werner systems could easily produce spurious results. Using wavelength anticoincidences in the occasional continuum windows in the PHL 957 Lyα forest, we were able to set a limit of $N(H_2) \leq 5 \times 10^{15}$ cm^{-2}, which corresponds to a value of the molecular fraction $f = N(2H_2)/N(H + H^+ + 2H_2) \leq 2 \times 10^{-6}$. Typical values of f in Galactic diffuse clouds with comparable column densities of H[N(H) $\approx 10^{20}$–

[1] Observations reported here were obtained with the Multiple Mirror Telescope, a joint facility of the Smithsonian Institution and the University of Arizona.

10^{21} cm^{-2}] lie between 0.05 and 0.5. We also searched for CO at the same redshift and set a limit of $N(\mathrm{CO}) \leq 4 \times 10^{13}$ cm^{-2}.

While research for the present paper was in progress, we found strong evidence for the presence of H_2 at $z = 2.811$ toward PKS 0528−250 (Foltz, Chaffee, and Black 1988, hereafter Paper IV). In our view, no other convincing evidence for H_2 or CO at early epochs exists, and the best limits suggest that both molecules are typically much less abundant than in Galactic clouds of comparable H column density.

Of course, the radiation environment strongly influences the abundances of H_2 and CO since both molecules can be destroyed readily by photons longward of the Lyman limit of H. In clouds of high column density and low ionization, molecules may still be able to form in detectable amounts.

In order to investigate absorption systems that may reveal conditions in the gaseous components of disk galaxies, we present below an analysis of a cloud of low ionization and high column density at $z = 1.776$ toward MC 1331+170, a QSO whose rich absorption line spectrum was first analyzed in detail by Carswell *et al.* (1975). The $z = 1.776$ system exhibits not only the damped Lyα absorption profile characteristic of Lyα disk systems, but absorption at 21 cm as well (Wolfe and Davis 1979). At this redshift, the principal H_2 features lie below 3000 Å, and we suggest that this system would be an excellent one in which to search for H_2 with the *Hubble Space Telescope*.

II. OBSERVATIONS AND REDUCTIONS

Spectroscopic observations of 1331+170 were obtained with the MMT spectrograph, and the journal of those observations is presented in Table 1. The spectral resolution is 1 Å (FWHM) for $\lambda \leq 5500$ Å and 2 Å for $\lambda > 5500$ Å. The data were flat-fielded and wavelength-mapped as described in Paper I. Figure 1 presents the resulting spectrum of 1331+170. All wavelengths and redshifts quoted or displayed in this paper are vacuum, heliocentric values. The measured magnitude of the 1 σ error is plotted along the abscissa, and the measured signal-to-noise ratio, S/N $\approx$ 80, at the peak of the Lyα emission line makes these the data of highest S/N we have ever obtained at this resolution with the MMT. Such high data quality is essential since we anticipate that many of the important spectral features will be weak.

III. LINE IDENTIFICATIONS AND COLUMN DENSITIES

Although at least five absorption line systems toward 1331+170 can be identified from our data, by far the strongest and richest is that at $z = 1.776$, and we report here only results relevant to that system. In order to identify its associated absorption lines, we have adopted a redshift $z_{\mathrm{abs}} = 1.77642$ inferred by Wolfe and Davis (1979) from the 21 cm absorption line. We compare the redshifted wavelengths of known atomic resonance lines that fall in our observational window with the measured wavelengths of all lines with equivalent width in the observer's frame $W_{\mathrm{obs}} > 100$ mÅ, the typical 3 σ value of our formal upper limit to the weakest measurable absorption feature. Our 1 σ uncertainty in the pixel-to-wavelength conversion is 0.3 Å in the observer's frame; if the measured feature lies within 4 σ of the predicted position of a known resonance line it is included as a probable identification.

Table 2 lists all lines so identified. Column (1) gives the observed wavelength, column (2) the ion proposed to be responsible for the observed line, column (3) the rest wavelength of the line, column (4) its observed equivalent width, and column (5) its oscillator strength. The column densities tabulated in column (6) are determined as described below. The recent astrophysical literature contains Si II oscillator strengths based on both an analysis of interstellar absorption lines (Shull, Snow, and York 1981; Van Buren 1986) and on elaborate ab initio calculations (Nussbaumer 1977; Froese Fischer 1981; Dufton *et al.* 1983). We have adopted the mean of the length and velocity forms of the oscillator strengths calculated by Dufton *et al.* (1983) for all transitions of Si II except for the weak $3p\ ^2P - 3s3p^2\ ^2D$ multiplet containing λ1808, for which we take $f = 0.003$, the upper bound of their empirical estimate.

The strong Lyα line identified in Figure 1 is easily resolved

TABLE 1

MC 1331+170: JOURNAL OF OBSERVATIONS

Date of Observation (1985)	Resolution (FWHM) Å	Wavelength Range Å	Integration Time (s)
Feb 16	1	3700–4500	1800
Mar 24	1	3150–4050	6000
Mar 24	1	3850–4750	6000
May 12	1	4475–5225	3600
May 19	2[a]	5500–6950	4800
May 20	1	4475–5225	4800
Jun 19	1	4700–5625	3600
Total:	...	...	30,600

[a] Obtained with the 832 grooves mm^{-1} grating in first order. All others obtained in second order.

TABLE 2

MC 1331+170 − $Z_{\mathrm{abs}} = 1.77642$ SYSTEM

λ_{obs} (1)	Ion (2)	λ_{rest} (3)	$W_{\lambda\mathrm{obs}}$ (4)	f (5)	N(cm^{-2})[a] (6)
3303.90.....	Si II	1190.42	1.04	0.285	4.6(14)
3312.03.....	Si II	1193.29	0.86	0.568	1.1(14)
3349.19.....	Si III	1206.51	2.87	1.66	8.5(16)
3375.56.....	H I	1215.67	69.03	0.4168	1.5(21)
3499.26.....	Si II	1260.42	1.75	1.119	3.5(15)
3546.17.....	C I	1277.25	<0.06	0.156	<1.0(13)
3614.96.....	O I	1302.17	1.39	0.0486	7.8(15)
3621.20.....	Si II	1304.37	1.23	0.0937	1.9(15)
3689.40.....	C I	1328.83	<0.04	0.0924	<1.0(13)
3704.93.....	C II	1334.53	1.88	0.118	4.5(16)
3708.26.....	C II*	1335.70	0.50	0.118	1.4(14)
3869.37.....	Si IV	1393.75	2.13	0.528	2.1(16)
3894.32.....	Si IV	1402.77	1.33	0.262	6.4(14)
4238.95.....	Si II	1526.71	1.37	0.1163	1.0(15)
4257.45.....	Si II*	1533.43	<0.06	0.158	<1.0(13)
4297.81.....	C IV	1548.19	2.22	0.190	3.1(16)
4304.95.....	C IV	1550.76	1.74	0.095	5.0(15)
4331.17.....	C I	1560.31	0.09	0.081	2.0(13)
4465.89.....	Fe II	1608.55	0.83	0.062	3.8(14)
4600.08.....	C I	1656.93	0.12	0.135	1.4(13)
4638.79.....	Al II	1670.79	1.41	1.88	4.2(13)
5019.53.....	Si II	1808.01	0.26	0.003	1.2(15)
5148.46.....	Al III	1854.72	0.35	0.539	8.8(12)
5149.88.....	Al III	1854.72	0.13	0.539	3.0(12)
5171.63.....	Al III	1862.79	0.22	0.268	1.0(13)
5172.74.....	Al III	1862.79	0.10	0.268	4.5(12)
5299.45.....	C III]	1908.73	<0.10	1.6(−7)	<7.2(18)
5626.36.....	Mg I	2026.48	<0.07	0.11	<6.5(12)
6276.97.....	Fe II	2260.75	<0.05	0.0028	<1.5(14)
6573.42.....	Fe II	2367.59	<0.07	0.000212	<2.3(15)
6593.07.....	Fe II	2374.46	1.02	0.0395	2.8(14)
6616.09.....	Fe II	2382.76	2.28	0.328	3.2(14)

[a] Calculated for $b = 30$ km s^{-1}.

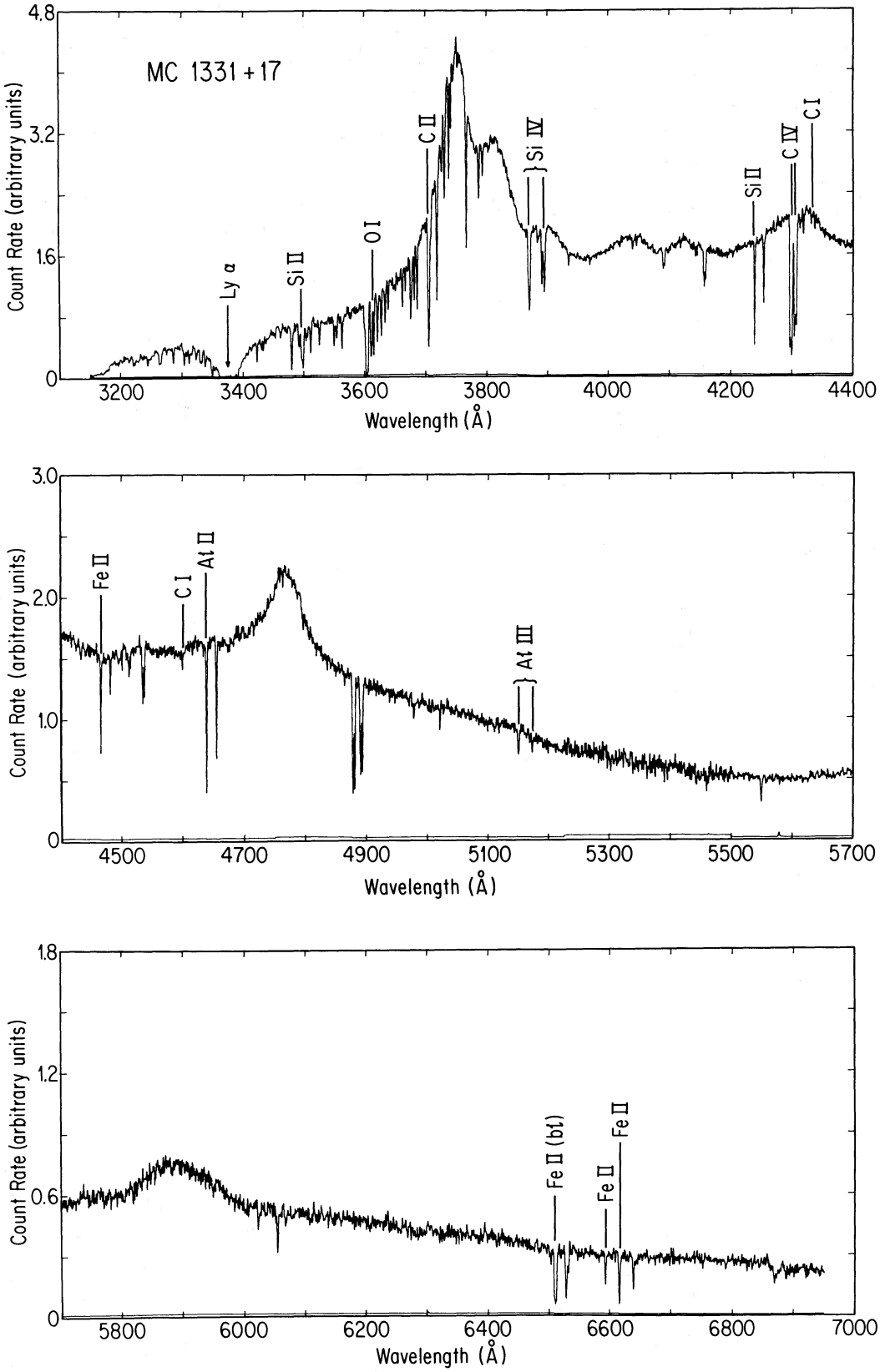

FIG. 1.—Composite MMT spectrum of MC 1331+170 at 1 Å resolution below 5500 Å and 2 Å resolution above. The emission line redsh.ft is ~2.08; thus prominent features near 3750, 3810, 4325, 4775, and 5875 Å correspond to emission by Lyα N v λ1240, Si IV λ1400, C IV λ1550, and C III] λ1909, respectively. Lines of various ions in the absorption system at $z = 1.776$ are identified. The lower spectrum is the rms noise level as derived from the counting statistics of the object, sky, and dark signals. The ordinate has been corrected for neither atmospheric extinction nor the wavelength-dependent sensitivity of the instrument.

by our data, so we can fit the profile with a Voigt function to determine the H I column density. Because the profile is damped, the inferred column density is independent of our choice of Doppler parameter. We infer $N(\mathrm{H}) = 1.5 \times 10^{21}$ cm^{-2} from the best fit to the data. An indication of the relative precision of the wavelength scale is the fact that the best-fitting wavelength of Lyα is within 0.35 Å (1.1 σ) of that predicted from the 21 cm redshift.

As frequently occurs in systems of high column density, the C IV absorption exhibits pronounced velocity structure, and the line listed in Table 2 is the middle component of a three-component blend ($z_{\mathrm{abs}} = 1.7750$, 1.7760, and 1.7774) only partially resolved in our data. To deduce the equivalent width of the appropriate line we fit a three-component Voigt profile to the data using software that minimizes χ^2 by adjusting N, λ, and b for each line. Other obvious blends were treated similarly.

The strengths of all metal lines are such that the usual degeneracy of solutions exists between Doppler parameter and column density, which can be broken in a number of ways. Since we have detected six lines of Si II and five of Fe II, we have chosen to construct an empirical curve of growth for those ions which is presented in Figure 2. Both yield $b = 30$ km s^{-1}, and we have adopted this Doppler parameter to infer the column density for all metal lines from their equivalent widths, including those of Si II and Fe II. Thus scatter in the column densities for Si II and Fe II reflects the scatter of the individual lines from the best-fit curve of growth shown in Figure 2. The discrepant column densities inferred from each line of the Si IV and C IV doublets suggest that the use of a single Doppler parameter for both low and high ionization states is almost certainly inappropriate.

The line of sight to 1331+170 displays neutral carbon absorption, which is seen only rarely and which can be used as a thermometer for measuring the radiation temperature of the microwave background radiation at this epoch (Meyer *et al.* 1986). We adopt a column density of C and a $^3P_0$–$^3P_1$ fine-structure excitation temperature, $T_{\mathrm{ex}}(C) < 16$ K, that are based on the results of Meyer *et al.* (1986).

No molecular absorption lines are identified in the spectrum. The strongest bands of the $A^1\Pi$–$X^1\Sigma^+$ system of CO, $\lambda = 1344$–1544 Å at rest, are not present at the level of $W_\lambda <$ 50–70 mÅ (2 σ) in the observed frame. The corresponding upper limit on column density, $N(\mathrm{CO}) < 1.1 \times 10^{13}$ cm^{-2}, is determined for a Doppler parameter $b = 10$ km s^{-1} with a curve of growth that accounts explicitly for the intrinsic line blending within the (2, 0) band when the rotational excitation temperature is taken to be $T_{\mathrm{rot}} = 7.5$ K, the background radiation temperature at this epoch. The band oscillator strengths for the CO A-X system are based on the transition moment function of Field *et al.* (1983). Because corrections made in manuscript were not actually incorporated into the published versions of Paper I, the CO oscillator strengths in Table II of that paper are all too small by a factor of 2. The corrected values appear in Table 3 of Paper II.

The ultraviolet lines of H_2 that arise in the ground vibrational state of the molecule all lie at rest wavelengths ($\lambda < 1130$ Å) too short for ground-based observations of this QSO. Lines of vibrationally excited H_2 that can be excited by ultraviolet pumping in interstellar clouds (see, e.g., van Dishoeck and Black 1986) are also absent. A line at 1369.58 Å (rest) that is often seen in Galactic diffuse clouds and that is attributed to the G(3d)–$X^2\Pi$ transition of CH (Black 1980) is not seen at the level of $W_{\mathrm{obs}} < 48$ mÅ (2 σ) in the spectrum of 1331+170.

IV. PHYSICAL CONDITIONS IN THE CLOUD AT $z = 1.776$

a) Atomic Constituents

Detectable amounts of carbon and silicon in three stages of ionization and measurements of (or limits on) excited fine structure absorption in C I and C II allow us to draw some qualitative conclusions concerning the physical conditions in the $z = 1.776$ cloud toward 1331+170.

Table 3 summarizes the column densities of relevant carbon

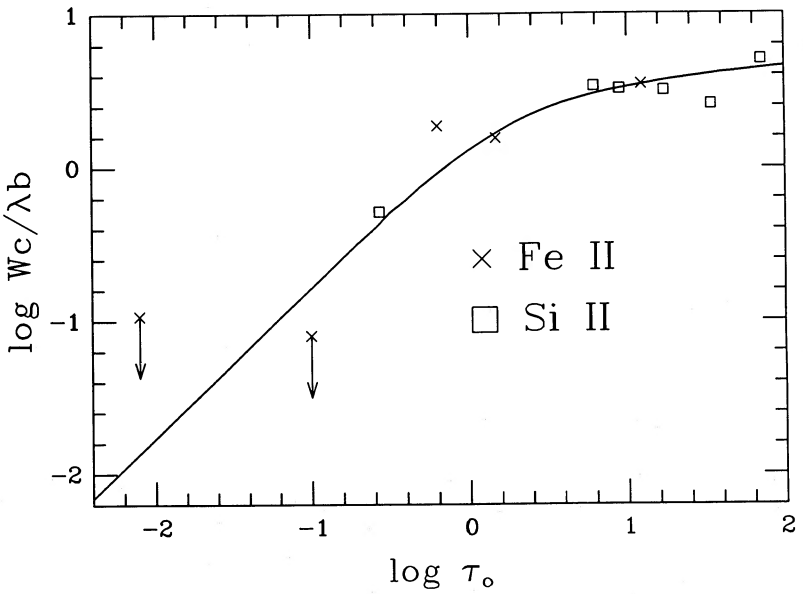

FIG. 2.—Curve of growth for lines of Fe II and Si II. The solid curve which best fits the data is the theoretical curve of growth for $b = 30$ km s^{-1}.

TABLE 3

CARBON AND SILICON IONIC COLUMN DENSITIES

Ion	$N_{b=50}$ (cm^{-2})	$N_{b=30}$ (cm^{-2})	Number of Lines
Si II	3.4(14)	1.3(15)	6
Si III	6.0(15)	8.5(16)	1
Si IV	3.1(14)	1.1(16)	2
C I	1.7(13)	1.8(13)	2
C II	1.4(15)	4.5(16)	1
C II*	1.2(14)	1.4(14)	1
C III	<7.2(18)	<7.2(18)	1
C IV	7.0(14)	1.8(16)	2

and silicon ions at $z = 1.77642$, where we have taken the simple average of the column density when more than one line of a given ion is present in Table 2. As mentioned above the discrepant values of $N(C^{+3})$ and $N(Si^{+3})$ suggest that the Doppler parameter derived for Si II and Fe II lines does not apply to the species of higher ionization; therefore, we present in Table 3 ionic column densities for $b = 50$ as well as for $b = 30$ km s^{-1}. The former value gives a self-consistent value of $N(C^{+3})$ for both lines of the doublet.

In order to restrict the number of free parameters in the analysis, we have used very simple photoionization models. In particular, no attempt has been made to describe the ionization and excitation of a large number of species in a properly stratified absorbing region. The resolution of existing data is inadequate to establish definitively whether the higher stages of ionization of carbon and silicon in fact occupy the same volume of space under the same conditions as the neutral hydrogen and the lower stages of ionization, although the inferred line widths and C IV profile structure strongly suggest that they do not.

Furthermore, the modest resolution of our data is inadequate to resolve any velocity structure that is likely to be present in the absorbing cloud. The 21 cm profile shows a dominant, low Doppler width component, but provides no guidance about how to parcel out the ionization structure over velocity. Thus, multicomponent models await the availability of higher resolution data that will allow us to better constrain the choice of model parameters. We take some solace in the work of Jenkins (1986) that suggests for interstellar clouds, single-component curves of growth still yield reasonably reliable column densities for ensembles of lines even when the true distribution of absorbers is far more complex.

Models have been computed as described in Paper II for a uniform cloud of kinetic temperature T and total density $n_H = n(H) + 2n(H_2) + n(H^+)$. The cloud is exposed to a radiation field of mean flux

$$\phi_\nu = \frac{4\pi I_\nu}{h\nu} = 3 \times 10^{-8} \phi_0 \left(\frac{\tilde{\nu}}{10^5}\right)^{-2} \text{ photons s}^{-1}\text{ cm}^{-2}\text{ Hz}^{-1},$$

where $\tilde{\nu} = \nu/c$ in cm^{-1} and ϕ_0 is a scaling factor such that $\phi_0 = 1$ recovers the mean flux of Galactic starlight at $\lambda = 1000$ Å ($\tilde{\nu} = 10^5$ cm^{-1}). Rather than treat the transfer of radiation and the stratification of ions in detail, the cloud is assumed to be opaque to radiation of frequencies between $\tilde{\nu}_L$ and $\tilde{\nu}_c$, where $\tilde{\nu}_L$ is the frequency of the Lyman limit of H and $\tilde{\nu}_c$ is an adjustable cutoff frequency: that is, $\phi_\nu = 0$ for $\tilde{\nu}_L \le \tilde{\nu} \le \tilde{\nu}_c$. As in Paper II, the steady state abundances of the principal forms of hydrogen, helium, and carbon are calculated. In addition, silicon in the form of Si, Si^+, Si^{+2}, Si^{+3}, Si^{+4}, and Si^{+5} is now treated similarly. Charge transfer processes involving hydrogen and helium are included in the ionization balance. The steady state concentrations of C, C^+, and Si^+ in the fine-structure levels of their ground terms are computed explicitly. The treatment of fine-structure excitation incorporates collisional excitation and de-excitation by electron- and hydrogen-atom impact, absorption and spontaneous and stimulated emission in the fine-structure transitions for an appropriate background radiation field, and radiative pumping through the strongest ultraviolet resonance lines.

The results of the simple cloud models are presented in Table 4. All these models were constructed to satisfy the following observational constraints: the column density of H, $N(H) = 1.5 \times 10^{21}$ cm^{-2}; the column densities of C^+ and C; and the lowest fine-structure excitation temperatures, $T_{ex}(C) < 16$ K and $T_{ex}(C^+) = 13.6$. Models A–D have $\tilde{\nu}_c \approx 10^6$ cm^{-1} and presume that all observed stages of ionization of carbon and silicon arise in the same physical region. Models E–H are computed for the case in which the Si III, Si IV, C III, and C IV absorption is assumed to arise outside the cloud that produces the absorption by H I, C I, C II, and Si II, and these models are constrained only by the observed column densities of the latter species. Generally speaking, $N(C^+)/n(C)$ is very sensitive to the value of ϕ_0/n_H while n_H is constrained by the value of $T_{ex}(C^+)$ for a given value of T. None of the principal observational constraints is very sensitive to temperature as long as $T > T_{ex}(C^+)$, although models such as E and F, with large $\tilde{\nu}_c$ and $T > 1000$ K, are ruled out by the observed limit on $T_{ex}(C)$.

If taken at face value, the tabulated value of $T_{ex}(C^+)$ provides a stronger constraint on the cosmic background radiation temperature than the limit on $T_{ex}(C)$ discussed by Meyer *et al.* (1986). This comparison should be made with great caution because the ground-level C II line is strongly saturated and the value of $T_{ex}(C^+)$ is thus subject to large uncertainties due to curve-of-growth effects. The much weaker C I lines are less susceptible to such uncertainties. For example, if we assume a single-component curve of growth and allow for an uncertainty of only ± 5 km s^{-1} in the adopted value of the Doppler parameter $b = 30$ km s^{-1}, then the corresponding uncertainty in the excitation temperature is $T_{ex}(C^+) = 14^{+5}_{-3}$ K. Thus the limit on the background radiation temperature allowed by the observed equivalent widths of C II lines is still less restrictive than that provided by the C I lines. With data of very high resolution and S/N, the fine-structure excitation of C II could, of course, yield interesting constraints.

Models A–D have low densities $n_H = 0.03$–0.8 cm^{-3} and fairly high ionization fractions, $n_e/n_H \approx 0.4$–1. The optical depth of the H Lyman continuum is $\tau_H \approx 2500$ at $\lambda 584$ Å when $N(H) = 1.5 \times 10^{21}$ cm^{-2}, thus we expect no measurable continuum flux in the vicinity of the He I resonance lines. However, helium is potentially observable in such clouds through absorption in the 2^3S–2^3P transition at $\lambda_{vac} = \lambda_0(1 + z) = 3.0077$ μm. The overall carbon and silicon abundances inferred from models B–D are 0.3 and 0.4–0.9 times their values in the solar photosphere, respectively. Predicted H_2 column densities are presented for two limiting cases as discussed in Paper II. The higher column density results from the adoption of an efficiency factor $y_f = 1$ for formation of H_2 on grain surfaces which is comparable to that in Galactic interstellar clouds. The lower H_2 abundances result from gas phase processes only ($y_f = 0$). If dust grains are present, the values of n_H and ϕ_0 are low enough in these models to make it likely that the equilibrium grain temperature remains sufficiently low for

TABLE 4

MC 1331+170 CLOUD MODELS

Property	A	B	C	D	E	F	G	H	Observed
n_H (cm^{-3})	0.043	0.031	0.037	0.81	16.0	40.0	9.9	2900	...
T^a	10000	1000	100	15	10000	1000	100	15	...
ϕ_0	0.26	0.97	1.61	78.5	0.28	0.98	0.11	46.0	...
$\tilde{v}_c$ (10^6 cm^{-1})	0.55	0.80	0.72	0.85	90	90	90	90	...
[C]/[H]	2.5(−5)	1.5(−4)	1.2(−4)	1.2(−4)	3.0(−5)	3.0(−5)	3.0(−5)	3.0(−5)	...
[Si]/[H]	4.5(−6)	4.1(−5)	1.9(−5)	4.0(−5)	8.7(−7)	8.7(−7)	8.7(−7)	8.7(−7)	...
N(H)^b	1.5(21)	1.5(21)	1.5(21)	1.5(21)	1.5(21)	1.5(21)	1.5(21)	1.5(21)	1.5(21)
N(He)^b	5.7(17)	1.5(18)	3.2(18)	8.3(18)	1.1(20)	1.1(20)	1.1(20)	1.1(20)	...
N(He$^+$)^b	7.0(19)	6.0(19)	6.1(19)	6.6(19)	4.7(11)	6.0(11)	2.0(11)	2.1(11)	...
N(H$_2$) $y_f = 1^b$	2.0(15)	1.2(14)	2.8(13)	4.8(12)	6.9(17)	1.6(17)	1.1(17)	2.9(16)	...
N(H$_2$) $y_f = 0^b$	2.6(13)	4.2(11)	7.5(10)	3.1(10)	1.2(16)	3.7(14)	3.1(13)	1.4(12)	...
$n(e)/n_H$	1.00	0.75	0.60	0.42	2.7(−3)	5.7(−4)	1.5(−4)	6.7(−5)	...
N(C)^b	1.8(13)	1.8(13)	1.8(13)	1.8(13)	1.8(13)	1.8(13)	1.8(13)	1.8(13)	1.8(13)
N(C$^+$)^b	4.5(16)	4.5(16)	4.5(16)	4.5(16)	4.5(16)	4.5(16)	4.5(16)	4.5(16)	4.5(16)
N(C^{+2})^b	1.8(17)	2.6(17)	2.0(17)	1.5(17)	negligible	negligible	negligible	negligible	<7(18)
N(C^{+3})^b	1.6(16)	2.1(16)	2.1(16)	1.9(16)	negligible	negligible	negligible	negligible	1.8(16)
N(Si)^b	1.3(11)	7.7(10)	9.7(10)	9.9(10)	1.2(11)	7.9(10)	9.6(10)	9.9(10)	...
N(Si$^+$)^b	1.3(15)	1.3(15)	1.3(15)	1.3(15)	1.3(15)	1.3(15)	1.3(15)	1.3(15)	1.3(15)
N(Si^{+2})^b	3.6(14)	4.8(14)	4.8(14)	7.8(14)	4.8(10)	9.8(9)	negligible	negligible	8.5(16)
N(Si^{+3})^b	3.0(15)	7.2(15)	6.6(15)	1.1(16)	negligible	negligible	negligible	negligible	1.1(16)
T_{ex}(C)^a	8.3	8.0	7.9	13.7	27.5	17.3	8.7	14.4	<16
T_{ex}(C$^+$)^a	14.1	14.1	14.1	14.1	14.1	14.1	14.1	14.1	14.1
T_{ex}(Si$^+$)^a	38.9	39.6	34.2	47.9	42.6	44.6	29.4	45.1	<74
W_λ(10833) (mÅ)	2.3	5.4	27.	1315.	negligible	negligible	negligible	negligible	...

[a] In degrees Kelvin.

[b] In cm^{-2}.

NOTES.—the notation 1(10) means 1×10^{10}. The excitation temperature listed for neutral carbon, T_{ex}(C), refers to the relative populations of the $^3P_0$ and $^3P_1$ fine-structure levels of the ground term only. The equivalent width of the He I λ10833 line is a rest value and it incorporates a correction for curve-of-growth effects at $b = 30$ km s^{-1}.

H_2 formation to be efficient even for the higher gas temperatures. There is no useful constraint on temperature in models A–D.

In models E–H, which exclude extreme ultraviolet (EUV) photons, the inferred densities are rather larger, $n_H \approx 10$–3000 cm^{-3}, while the fluxes of 1000 Å photons remain low, $\phi_0 \approx 0.1$–50. The carbon and silicon abundances in models E–H are 0.06 and 0.02 times their solar photospheric values, respectively. These abundances [or equivalently, the observed column density ratios $N(C^+)/N(H)$ and $N(Si^+)/N(H)$] can be taken as lower limits to their true values. Temperatures greater than 1000 K (models E and F) are excluded by the value of T_{ex}(C).

b) *Molecular Constituents*

For models E–H with dust grains, molecular hydrogen is predicted to be present at levels that should be readily detectable with the High-Resolution Spectrometer on HST. In contrast, the most optimistic assumptions in Models A–D yield small amounts of H_2. If $y_f = 1$, the computed values of $N(H_2)$ must still be considered underestimates because these models did not allow for effects of self-shielding against dissociating photons.

In order to assess the possibility of detecting H_2, we have calculated synthetic spectra similar to those described in Paper IV for a range of values of $N(H_2)$. Owing to the relatively low redshift of the $z = 1.776$ system, its Lyα forest should be considerably less cluttered than those observed from the Earth's surface toward higher redshift QSOs, and we have also calculated a synthetic Lyα forest with the appropriate line density and equivalent width distribution in the region of the strongest predicted H_2 lines.

These results are presented in Figure 3, where panel *d* is the simulated Lyα forest and panels *a*, *b*, and *c* are the synthetic H_2 spectra at various column densities. The resolution is 15 km s^{-1}, and we have added noise to the simulations to mimic an observed S/N ≈ 20.

We estimate that if the Lyα forest toward MC 1331+170 is as sparse as shown in Figure 3*a*, a column density of H_2 as small as 10^{14} cm^{-2} should be detectable with the High Resolution Spectrometer on HST.

Setting an upper limit on the molecular hydrogen column density of 10^{14} cm^{-2} would considerably limit the range of models in Table 4 that would then satisfy all observational constraints. Of the models with $y_f = 1$ only models C and D would be acceptable; of those with $y_f = 0$, only models E and F would be eliminated. Detection of molecular hydrogen would provide a determination of the rotational excitation temperature, which could be used as a constraint on the kinetic temperature of the gas, a physical parameter that is otherwise poorly established.

The existing limits on CO in the QSO absorbing regions are much smaller than the amount observed in the ζ Oph cloud, although the observed CO abundance in the latter is unusually large for a diffuse cloud with $N(H) \lesssim 10^{21}$ cm^{-2}. The smallest amount of CO detected in a Galactic diffuse cloud is $N(CO) = 1.2 \times 10^{12}$ cm^{-2} toward π Sco (Federman *et al.* 1980; corrected for improved oscillator strengths), where $N(H_2) = 2.1 \times 10^{19}$ cm^{-2}. Moreover, this is the cloud of smallest H_2 column density in which CO is also seen, if the possible

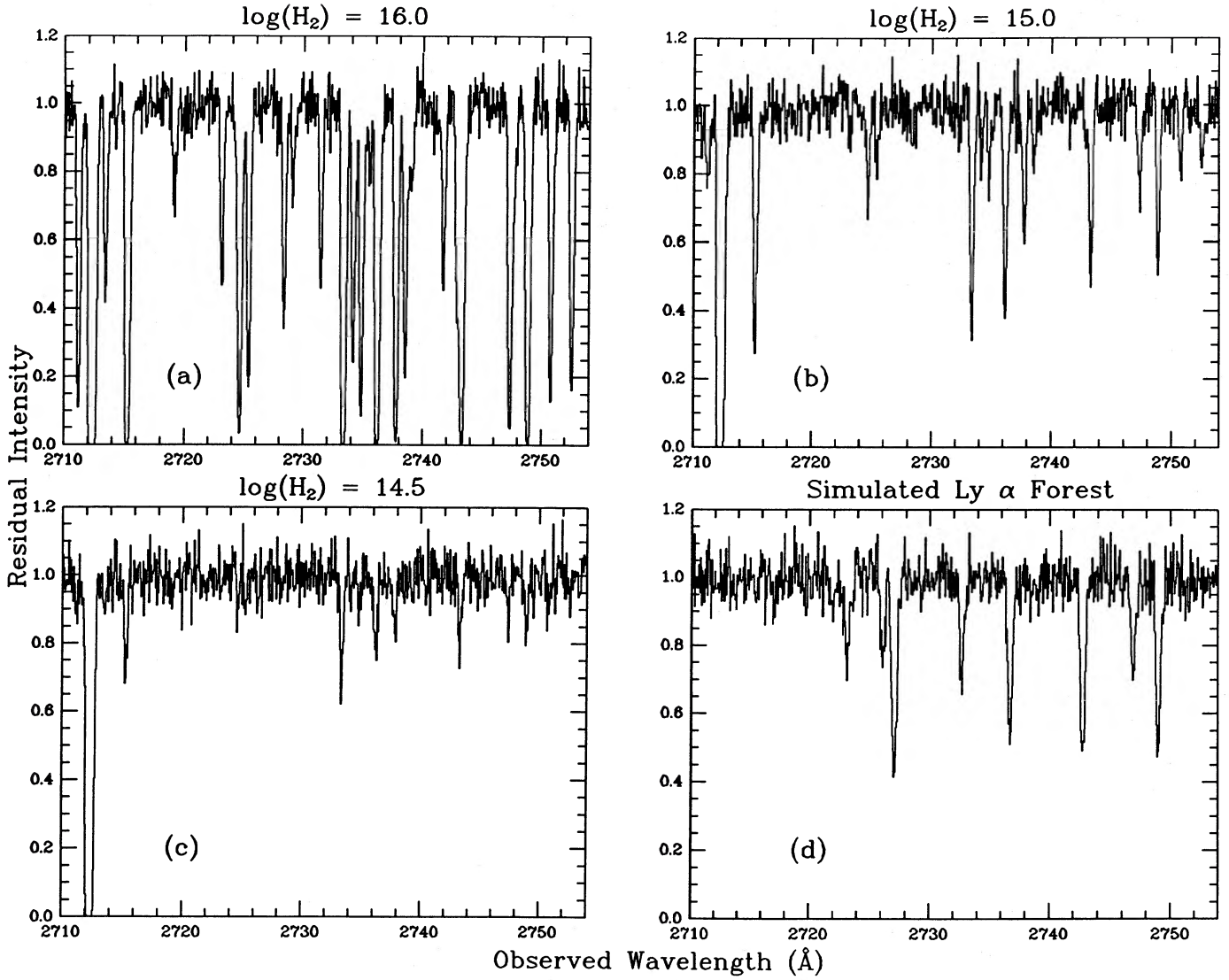

FIG. 3.—Synthetic spectra of the absorbing cloud toward 1331+170 in the rest wavelength region between 976 and 991 Å. (*d*) Simulated absorption by Lyα and Lyβ lines from systems of the Lyα forest at other redshifts. The others (*a–c*). The expected H_2 absorption for H_2 column densities of (*a*) 10^{16}, (*b*) 10^{15}, and (*c*) $10^{14.5}$. The strong feature at 2712 Å in the H_2 simulations is the expected position and strength of C III λ977 Å at $z = 1.776$. The simulation were calculated for S/N = 20 and $\lambda/\Delta\lambda = 20{,}000$. Based on the known continuum flux of 1331+170 in this spectral region and the advertised sensitivity of the High Resolution Spectrometer on HST, spectra of this quality should be obtainable in $\sim$20 hr of exposure time.

detection of CO with $N(CO) = 4 \times 10^{12}$ cm^{-2} toward ι Ori where $N(H_2) = 4.9 \times 10^{14}$ cm^{-2} is considered to be spurious. CO, like H_2, can be dissociated by photons at $\lambda \approx 1000$ Å, but can also shield itself effectively once a threshold column density has been built up. The column of H_2 at which the CO begins to occupy a significant fraction of the gas phase carbon is $N(H_2) \approx 10^{21}$ cm^{-2} in Galactic clouds. However, the column density of H_2 at which the CO becomes detectable [$N(CO) \gtrsim 10^{13}$, say] is very sensitive to details (van Dishoeck and Black 1988) and cannot be predicted without much tighter constraints on the physical conditions and on the abundance and excitation of H_2. It is not impossible, however, that the PKS 0528−250 cloud that apparently supports $N(H_2) = 10^{18}$ cm^{-2} also contains a measurable column density of CO.

As mentioned above, the data provide hints that the lines of more highly ionized species arise in regions of different conditions than those of H I, C I, C II, and Si II, in which case models E–H are to be preferred to models A–D. Considerations of internal consistency also enter the choice between the two types of models. Models A–D require significant radiation at frequencies $\tilde{\nu} \gtrsim \tilde{\nu}_c \approx 10^6$ cm^{-1} at which the opacities due to continuous absorption by H, He, and He^+ must be large, $\tau(\tilde{\nu}_c) \approx 23$–93, if the absorption is attributed to a single "cloud." Thus a physical interpretation of these models suggests that the absorption arises in a large number ($\gtrsim$20) of condensations each of which contains a corresponding fraction of the total column density, has a fully irradiated surface, and has $\tau(\tilde{\nu}_c) \approx 1$. The relatively small velocity dispersion, $b = 30$ km s^{-1}, determined from the Si II and Fe II absorptions would place strong constraints on the kinematics of such a system of cloudlets. In models E–H, on the other hand, the more highly ionized species and the more energetic photons are simply assumed to lie elsewhere along the line of sight. More detailed comparison of line profiles for C II and C IV lines at higher resolution could help resolve this uncertainty about the distribution of absorbers. The detection of H_2 lines at $z = 1.776$

TABLE 5

COMPARISON OF QSO ABSORBING CLOUDS AND A GALACTIC CLOUD

Property	MC 1331+170[a] ($z = 1.776$)	PHL 957[b] ($z = 2.309$)	PKS 0528−250[c] ($z = 2.811$)	ζ Oph[d] ($z \sim 0$)
N(H) (cm^{-2})	1.5×10^{21}	2.5×10^{21}	1.3×10^{21}	5.2×10^{20}
$N(H_2)$ (cm^{-2})	...	$<5 \times 10^{15}$	10^{18}	4.2×10^{20}
$N(C^+)$ (cm^{-2})	4.5×10^{16}	7.8×10^{15}	...	9.3×10^{16}
N(CO) (cm^{-2})	$<1.1 \times 10^{13}$	$<4 \times 10^{13}$	...	2.0×10^{15}
T_{ex}(C) (K)	<16	17.2	...	13.
$T_{ex}(C^+)$ (K)	14.1	...	...	17.
n_H (cm^{-3})	0.03–3000	1–6	...	350
T (K)	15–10^4	40–4000	100	30–100
ϕ_0	0.1–40	6–30	...	3.5
[C]/[H]	$(0.3–1.5) \times 10^{-4}$	4×10^{-6}	...	3×10^{-4}

[a] This work.
[b] Paper II.
[c] Paper IV.
[d] van Dishoeck and Black 1986 and references therein; the inferred parameters refer specifically to model G of that work.

would provide indirect support for the low-ionization models, although failure to detect H_2 would be inconclusive, because its abundance depends on unknown properties of grains.

c) *Comparison with a Galactic Interstellar Cloud*

It is instructive to compare some observed and inferred properties of three QSO "disk absorption systems" and of a well-studied diffuse interstellar cloud in the Galaxy. Such a comparison is presented in Table 5. Although the H column densities in the three QSO systems are similar and 3–5 times larger than in the reference Galactic cloud, some of their other properties differ significantly. In particular, the carbon abundance at $z = 1.776$ in 1331+170 may be comparable to local interstellar values while that in PHL 957 is clearly much lower. The H_2 abundance apparently differs by orders of magnitude between PKS 0528−250 and PHL 957. As discussed in Papers II and IV, the absence of H_2 in PHL 957 and its probable presence in PKS 0528−250 are governed at least partly by the value of ϕ_0/n_H. In PHL 957 $\phi_0/n_H \approx 1$–5 while for the Galactic cloud $\phi_0/n_H = 0.01$. In the case of 1331+170, the value of this parameter lies in the range 0.01–0.02 for Models E–H. The analysis indicates that the 1331+170 absorbing region is thus similar in several ways to Galactic diffuse clouds, provided that the highly ionized species arise in a physically distinct region from the less ionized ones.

V. CONCLUSIONS

We have examined the physical conditions likely to obtain in a high column density [N(H) = 1.5×10^{21} cm^{-2}] Lyα disk absorption region at $z = 1.776$ toward MC 1331+170.

The range of allowed simple physical models is constrained by observations of, and column densities inferred from, absorption lines of six metallic species at the same redshift as the hydrogen absorption. In particular, observations of lines from three ions of both Si and C allow us to limit the values of matter and radiation density that are in harmony with the observations. The observations further suggest that high and low ionization species are formed in physically distinct regions at $z \approx 1.776$.

Our best estimates are that the matter density in the low ionization region of the cloud lies in the range $10 \lesssim n_H \lesssim 3000$ cm^{-3} and that the radiation density at 1000 Å is similar to that seen by diffuse clouds in the Galaxy. The large range of allowed densities results because the temperature is poorly constrained within the range $15 \lesssim T < 1000$ K.

The absence of observable CO at 10 times less than the Galactic value provides no significant constraint on the physical conditions, although it may do so when better data on other species become available.

We suggest that the detection of molecular hydrogen at a column density $\gtrsim 10^{14}$ cm^{-2} would severely constrain the models and could provide the first clear evidence for dust in these systems. Such observations await the launch of the Space Telescope.

This work has been supported in part by the National Science Foundation through grant 87-00741 to the University of Arizona. E. F. van Dishoeck is thanked for comments.

REFERENCES

Aaronson, M., Black, J. H., and McKee, C. F. 1974, *Ap. J. (Letters)*, **191**, L53.
Black, J. H. 1980, in *Interstellar Molecules*, ed. B. H. Andrew (Dordrecht: Reidel), p. 257.
Black, J. H., Chaffee, F. H., Jr., and Foltz, C. B. 1987, *Ap. J.*, **317**, 442 (Paper II).
Carswell, R. F., Hilliard, R. L., Strittmatter, P. A., Taylor, D. J., and Weymann, R. J. 1975, *Ap. J.*, **196**, 351.
Chaffee, F. H., Jr., Foltz, C. B., and Black, J. H. 1986, *Soviet Astr. Letters*, **12**, 343 (Paper I).
Dufton, P. L., Hibbert, A., Kingston, A. E., and Tully, J. A. 1983, *M.N.R.A.S.*, **202**, 145.
Federman, S. R., Glassgold, A. E., Jenkins, E. B., and Shaya, E. J. 1980, *Ap. J.*, **242**, 545.
Field, R. W., Benoist, d'Azy, O., Lavolee, M., Lopez-Delgado, R., and Tramer, A. 1983, *J. Chem. Phys.*, **78**, 2838.
Foltz, C. B., Chaffee, F. H., Jr., and Black, J. H. 1988, *Ap. J.*, **324**, 267 (Paper IV).
Froese Fischer, C. 1981, *Phys. Scripta*, **23**, 38.
Jenkins, E. B. 1986, *Ap. J.*, **304**, 739.
Levshakov, S. A., Khersonskiĭ, V. K., and Varshalovich, D. A. 1986, *Soviet Astr.*, **30**, 16.
Meyer, D. M., Black, J. H., Chaffee, F. H., Jr., Foltz, C. B., and York, D. G. 1986, *Ap. J. (Letters)*, **308**, L37.
Nussbaumer, H. 1977, *Astr. Ap.*, **58**, 291.
Shull, J. M., Snow, T. P., and York, D. G. 1981, *Ap. J.*, **246**, 549.

Van Buren, D. 1986, *Ap. J.*, **311**, 400.
van Dishoeck, E. F., and Black, J. H. 1986, *Ap. J. Suppl.*, **62**, 109.
———. 1988, *Ap. J.*, submitted.
Varshalovich, D. A., and Levshakov, S. A. 1982, *Comments Ap.*, **9**, 199.
Wolfe, A. M., and Davis, M. M. 1979, *A.J.*, **84**, 699.
Wolfe, A. M., Turnshek, D. A., Smith, H. E., and Cohen, R. D. 1986, *Ap. J. Suppl.*, **61**, 249.

JOHN H. BLACK: Steward Observatory, University of Arizona, Tucson, AZ 85721

FREDERIC H. CHAFFEE, JR., and CRAIG B. FOLTZ: Multiple Mirror Telescope Observatory, University of Arizona, Tucson, AZ 85721-0465.